Archives of Materials Science and Engineering

Volume 61
Issue 2
June 2013
Pages 77-86

International Scientific Journal
published monthly by the
World Academy of Materials
and Manufacturing Engineering

Comparison between direct and indirect measurement methods for bulge tests

E.P. Marinho*, A.M. Silva Jr., G.F. Batalha
Laboratory of Manufacturing Engineering, Polytechnic School of Engineering,
University of Sao Paulo, Brazil
* Corresponding e-mail address: erickfalcone@gmail.com

Received 17.03.2013; published in revised form 01.06.2013

ABSTRACT

Purpose: To reinforce the standardization of the bulge test measuring procedures by comparison of two different bulge forming measurement methods.

Design/methodology/approach: Two different bulge forming measurement methods are used simultaneously in order to reinforce the standardization of the bulge test measuring procedures. An indirect method, Digital Image Correlation (DIC), is compared with a direct one, ultrasound pulse-echo method.

Findings: The main conclusion is that the DIC system is a valid indirect measurement method to study bi-axial sheet metal forming.

Research limitations/implications: The constant pressure bulge test method was used and it yielded positive results for comparing the direct and indirect method (considering thickness measurement of the bulge dome), as an important research implication is that the touch less measurement method could be applied to other sheet metal forming processes.

Practical implications: Tension tests are used as a standard accepted procedure to determine material parameter values for characterizing the forming sheet behaviour. However, by using a tension test, only a limited strain range can be considered for determining the true stress – true strain curve. Based on this limitation, the bulge test is used to achieve a much larger strain range under bi-axial loading conditions.

Originality/value: An indirect method, Digital Image Correlation (DIC), is compared with a direct one, ultrasound pulse-echo method, in situ, real time and on the same specimen.

Keywords: Digital Image Correlation; Ultrasound; Bulge test; Instrumentation; Sheet metal forming

Reference to this paper should be given in the following way:

E.P. Marinho, A.M. Silva Jr., G.F. Batalha, Comparison between direct and indirect measurement methods for bulge tests, Archives of Materials Science and Engineering 61/2 (2013) 77-86.

PROPERTIES

1. Introduction

Blow forming process is one of the most important and widely used forming methods in recent years. In this process, gas pressure is imposed over a sheet to make it flow into a die of the desired shape. For example, to produce maximum ductility in the SPF process case, it is desirable to adjust the forming pressure to keep the strain rate within an optimum range throughout the whole forming process [1].

Tension tests are used as a standard accepted procedure to determine material parameter values for characterizing the forming sheet behaviour [2],[3]. However, by using a tension test, only a limited strain range can be considered for determining the

true stress - true strain curve. Based on this limitation, the bulge test is used to achieve under bi-axial loading conditions much larger strain range. The sheet metals under biaxial tension can withstand much higher strain levels without local necking or fracture than in the tensile testing [4].

In this regard, the bulge test was proposed by Cheng et al [5], in which a thin circular plate is clamped by a hydraulic press and argon pressure gas is applied; the sheet is deformed assuming a semi-spherical shape. The dome height, h, is measured using an LVDT device as a function of time, geometric relationships relate pressure with stress, and stress-strain rate curves are obtained.

Analytical models for bulge forming were proposed considering the thickness variation in bulged shapes [6-8]. Although the analytical and experimental results were reasonable, there is no agreement about how suitable they are to predict the thickness, as in the uniaxial tensile test. Thus, to check whether a model reproduces an actual test is necessary to develop an instrumented biaxial test, in which specific parameters are obtained from the test in situ, real time and from the same specimen.

In this paper, a bulge test of a Pb-Sn alloy was conducted at room temperature. During the test, the bulge topography is continuously recorded using an ARAMIS 3D optical measurement system [9] while the dome height is also continuously measured with an ultrasonic pulse-echo technique [10].

Ultrasound is known to be an accurate and reliable measuring method. Measurements can be achieved by transmitting a sound pulse into just one side of a material and capturing the echo which arrives from the pulse reflection on the back-wall. The ultrasound pulse-echo is an interesting method to measure the dome height during the bulge test. On-line ultrasonic thickness measurement should/can provide a proper comparison and improve the understanding of the forming process.

Firstly the indirect measurement system and the direct one are presented; the former is a digital image correlation system and the latter is the ultrasound pulse-echo method.

2. Indirect Measurement System (IMS)

2.1. Summary description of IMS

The control system project is divided into tracking variables: Strain measurement and pressure measurement. In order to analyse thickness reduction through strain measurement, this system was already used to make a comparison between experimental measurements of the dome thickness reduction and the two analytical predictions using equations [11].

Fig. 1 shows the experimental setup and the schema used to measure the strain and the pressure.

In summary, the acquisition system works to guarantee pressure monitoring. The intention here is to analyse thickness reduction; thus, the forming pressure applied was constant; this setup is able to apply a forming pressure curve responsible for maintaining the strains rate constant, for example.

2.2. Selected system for strain measurements

The strain measurement was carried out employing the optical measurement system GOM-ARAMIS. The recorded data was compiled and critically analyzed.

The measurement system used to analyse the strain time evolution of a bulge test uses the three-dimensional optical measurement system (GOM-ARAMIS). This system provided 3D Optical analyses of PbSn 60-40 sheet forming, with high temporal resolution, as well as high accuracy, and its measure results are the 3D coordinates of position; it is described from the calibration steps to the application of this system to measure the thickness time reduction under biaxial fluid static expansion.

a)

b)

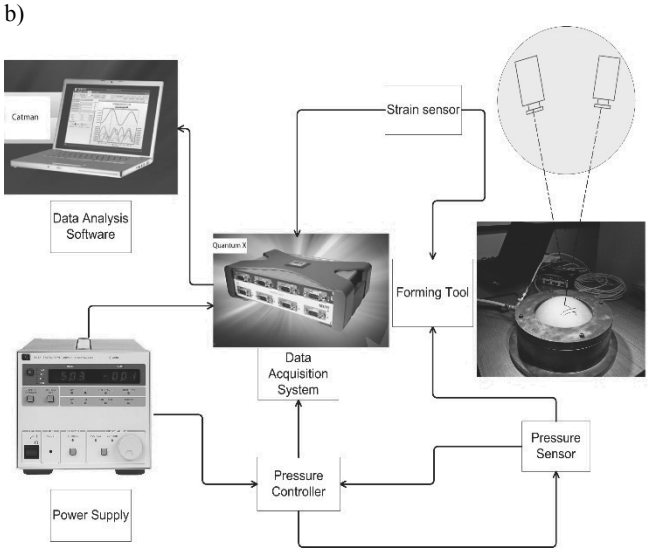

Fig. 1. a) Experimental Setup and b) Control instrumentation schema

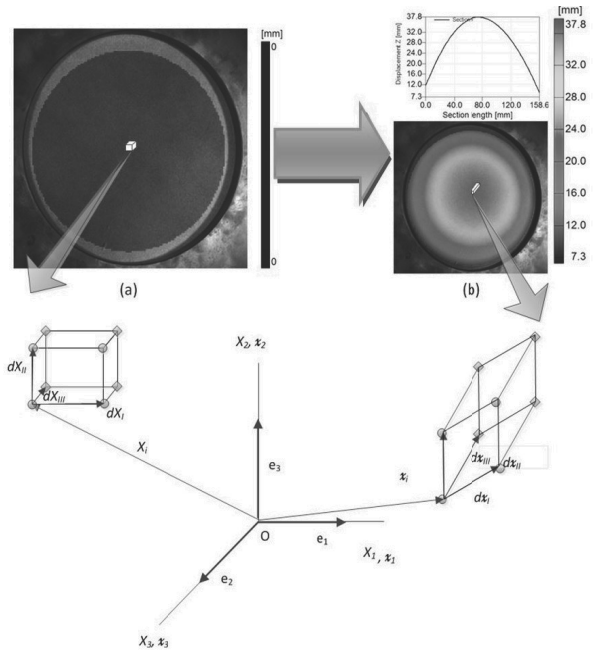

Fig. 2. Definition of a continuum body

Nevertheless, Digital Image Correlation based systems only observe surfaces of specimens or components. For determining a 3D deformation state, information about a material point behind the target surface is necessary. Due to this, the material behaviour in the thickness direction has to be assumed.

Consider the theory under an infinitesimal continuum body in a 3-dimensional Euclidean space at different moments, (a) at the beginning of the forming process and (b) at some stage before breaking time. In Fig. 2, the position of its particles in the beginning of the forming process is described by vector Xi, which refers to the position of particle i in the current configuration.

Following this nomenclature, some aspects of the bases used in ARAMIS to calculate the strains are presented.

2.3. Fundaments and notation employed on the bases of strain measurement at GOM-ARAMIS

In the ARAMIS system software, the nomenclature used for the variables follows the German convention, as can be seen also in the work by Vulcan [1]: Engineering strain: εand true strain: φ

Strain is the measure for the deformation of a line element and can be defined as [11]:

$$\lambda = \lim_{n \to 0} \left(\frac{l + \Delta l}{l} \right)^n \tag{1}$$

The stretch ratio λ is the relative elongation of an infinitesimal line element. A strain value ε can be defined as the function of stretch ratio λ.

The following known functions are frequently used strain measures:

- Technical strain:

$$\varepsilon^T = f(\lambda) = \lambda - 1 \tag{2}$$

- Logarithmic or true strain:

$$\varepsilon^L = \varphi = f(\lambda) = ln(\lambda) \tag{3}$$

- Green's strain:

$$\varepsilon^G = f(\lambda) = \frac{1}{2}(\lambda^2 - 1) \tag{4}$$

2.4. Deformation Gradient Tensor and x-y Strain Values

The deformation gradient tensor transforms a line element dX into the line element dx. In both cases, the line element connects the same material coordinates.

Thus, the deformation gradient tensor, Fig. 3. is defined as:

$$dx = F.dX \tag{5}$$

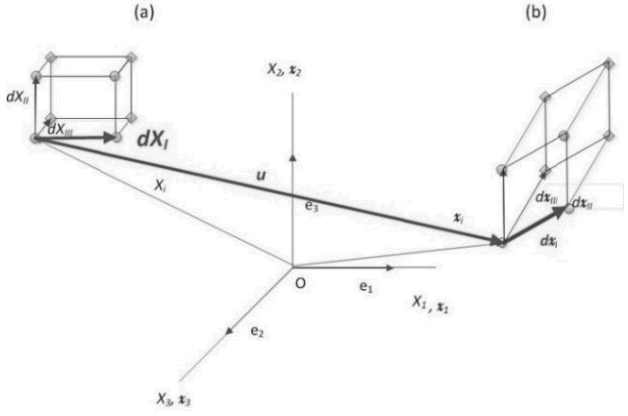

Fig. 3. Translation (u) and strain of a line element

In order to calculate the x-y Strain Values, it is necessary to separate the deformation gradient tensor in purely rotation matrix and pure stretch tensor.

$$F = R.U \tag{6}$$

$$F = V.R \tag{7}$$

The multiplicative decomposition of a constant tensor, equation (6) can be regarded as a sequence of two homogeneous deformations U, followed by R. Similarly, equation (7) is R followed by V. Here: Rotation R, right stretch tensor U and left stretch tensor V.

Values ε_ξ, $\varepsilon_{v\,e}$ ε_{xy} can directly be read from the symmetric stretch tensor U as follows [13]:

$$U = \begin{pmatrix} U_{11} & U_{12} \\ U_{21} & U_{22} \end{pmatrix} = \begin{pmatrix} 1+\varepsilon_x & \varepsilon_{xy} \\ \varepsilon_{xy} & 1+\varepsilon_y \end{pmatrix} \tag{8}$$

For the geometrical interpretation of values $\varepsilon_{xy,}$ shear angle γ_{xy} is used (Fig. 4). This angle describes the change of an angle of 90° in the undeformed state to a new angle in the deformed state.

$$\gamma_{xy} = \gamma_x + \gamma_y \tag{9}$$

$$\gamma_x = \arctan\left(\frac{\varepsilon_{xy}}{1+\varepsilon_x}\right) \tag{10}$$

$$\gamma_y = \arctan\left(\frac{\varepsilon_{xy}}{1+\varepsilon_y}\right) \tag{11}$$

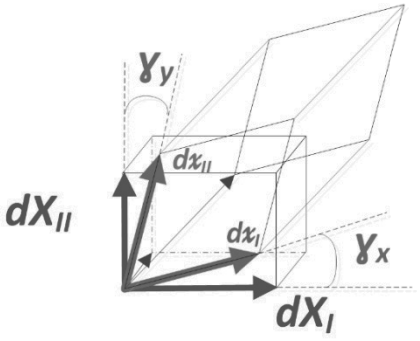

Fig. 4. Shear angle definition

The deformation gradient tensor F creates a functional connection of the coordinates of the deformed points P_d with the coordinates of the undeformed points P_u. [13].

$$P_{v,i} = u_i + F.P_{u,i} \tag{12}$$

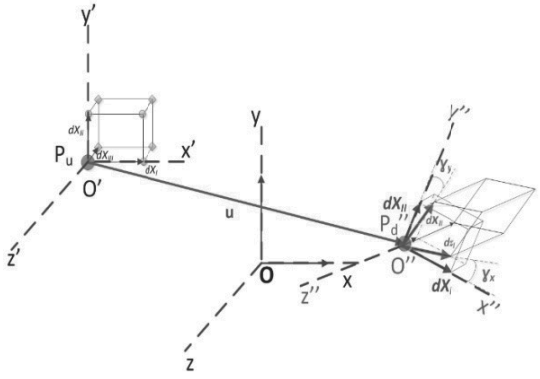

Fig. 5. Definition of the coordinate system (based on the deformation of a unit square)
x-y: Global coordinate system;
x -y : Local undeformed coordinate system;
x -y : Local deformed coordinate system = directions of strain.

The coordinates of the point (e.g. P_u and P_v) are calculated in the global x-y coordinate system. For the 2D discussion, the coordinate system x'-y' is parallel to x-y, but is placed in the undeformed position of the point of interest $P_{u,i.}$ The rotation matrix R defines the rotation from the x'-y' to the x''-y'' system. The coordinate system x''-y'' for the strain calculation is independent from the rigid body movement and rotation. It shows the deformation introduced by the stretch tensor U and defines the direction of the strain values. This leads to:
X'' direction = direction of strain x
Y'' direction = direction of strain y

2.5. Major and minor strain derived from the deformation gradient tensor

Some assumptions of material behaviour are necessary to complete the 3D study; based on the measure data, tow columns of F can be computed, and symmetrical matrix U can be transformed into the main diagonal form. The two eigenvalues, λ_1 and $\lambda_{2,}$ can be calculated as follows:

$$\lambda_{1,2} = 1 + \frac{\varepsilon_x + \varepsilon_y}{2} \mp \sqrt{\left(\frac{\varepsilon_x + \varepsilon_y}{2}\right)^2 - (\varepsilon_x.\varepsilon_y - \varepsilon_{xy}{}^2)} \tag{13}$$

R is proper orthogonal, satisfies (14) and (15) and, therefore, represents a rotation. To see this, note that U is symmetric and, therefore, satisfies (16) and (17), so that (18):

$$R.R^T = R^T.R = I \tag{14}$$

$$\det(\mathbf{R}) = 1 \tag{15}$$

$$U^{-T} = U^{-1} \tag{16}$$

$$U = (F^T.F)^{\frac{1}{2}} \tag{17}$$

$$R^T.R = (F.U^{-1})^T.(F.U^{-1}) = U^{-T}.F^T.F.U^{-1} = U^{-1}.U^2.U^{-1} = I \tag{18}$$

U can be expressed by (19) where $u^{(i)}$ are the three (mutually perpendicular) eigenvectors of U, and λ are the three Eigenvalues.

$$U = \lambda 1.u^{(1)} \otimes u^{(1)} + \lambda 2.u^{(2)} \otimes u^{(2)} + \lambda 3.u^{(3)} \otimes u^{(3)} \tag{19}$$

However, based on 2D Strain Computation, we obtain the square of the major and minor stretch, ε_1 and ε_2, of the volume element, λ_3 depends on the assumptions made about the material behaviour. By setting $\lambda_3 = 1$, a plane strain situation is assumed, for incompressibility equation (20) holds. For orthogonal material behaviour, equation (21) is valid. The assumption in the thickness direction allows calculating the missing vector and the determination of a full 3D deformation gradient [14].

$$\lambda 3 = \frac{1}{\sqrt{\varepsilon_1}.\sqrt{\varepsilon_2}} \tag{20}$$

$$\lambda 3 = \sqrt{\varepsilon_2} \tag{21}$$

The deformation gradient tensor describes the linear mapping between the corresponding vectors. This relationship must hold for any vector within this reference space. Two of the vectors can be calculated from measured data in both configurations. This allows the calculation of six out of nine unknowns of F. The third vector must not lie within the tangential surface. Otherwise, the linear dependence of the vectors appears which leads to an unsolvable problem. Because of this, one has to assume the material behaviour in thickness direction. The missing vector can be defined as:

$$dX_{III} = \frac{dX_{II} \times dX_I}{\|dX_{II} \times dX_I\|}.t \tag{22}$$

Where: t is the vector length projected on the thickness direction. dX_{III} should not be longer than the initial material thickness. Similarly, the vector in the thickness direction of the current configuration can be defined as:

$$dX_{III} = \frac{dX_{II} \times dX_I}{\|dX_{II} \times dX_I\|}.\lambda 3 \tag{23}$$

Where λ_3 is the stretch of the vector dX_{III}. This definition means that no shear deformation in the thickness direction occurs; in fact, this is only true for the infinitesimal vector length and shear stiff core of the material [13].

Without determining a strain value, the relationship between the stretch ratios can be expressed more generally. The volume constant can be defined as follows [15]:

$$\lambda_1.\lambda_2.\lambda_3 = 1 \tag{24}$$

2.6. Definition of the x-y Strain Values and the Strain Directions in 3D

The description so far showed the calculation of strain in 2D in detail. However, the measurement data in general consist of 3D points of the specimen surface.

The local strain coordinate systems must be tangential to the local surface, and for the strain calculation, the 3D data must be transformed into the 2D space [11].

In general, both directions (x' and y') are not parallel to the global coordinate system. This is shown in Fig. 6. The dashed lines are parallel to the x-z plane and the different local y' directions are tangential to the surface. Based in Fig. 5, the geometry of the parallelogram, together with the stretch tensor (γ_x and γ_y), defines the local strain directions (x'' and y'') in the deformed state.

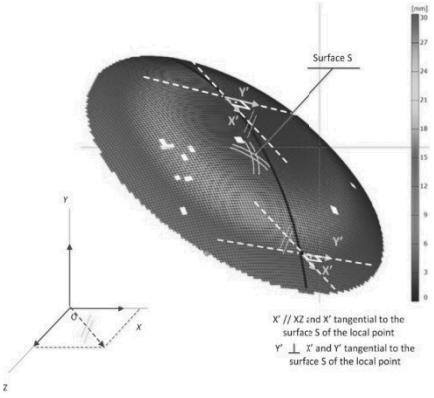

Fig. 6. Definition of the undeformed local surface strain coordinate system in 3D based on a plane parallel to x-z

2.7. Theoretical principle of the ARAMIS optical measuring

The principle is Photogrammetry - Fig. 7. The method is based on the correspondence between the distribution of grey level pixels of a rectangular area (facet) undeformed and deformed condition located under the 3D surface.

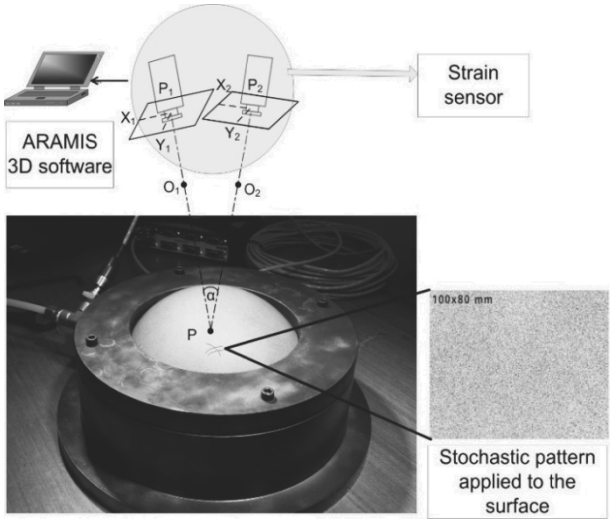

Fig. 7. Photogrammetry measuring principle and a 3D measuring arrangement

O_1 and O_2 are the perspective centres; point P is recorded by the CCD cameras in coordinates (x_1, y_1) and (x_2, y_2). To use the photogrammetric measurement, it is necessary to connect the camera image-coordinates and the object coordinates. Central projection is used to relate the pixels coordinates with images from the cameras and object coordinates. Fig. 7 shows how the central projection maps and one object-point onto the camera image. Object-point P is projected through a perspective centre O onto the projection plane of the camera.

The function connection between image- and object-coordinates, the so-called condition of collinearity, is given by the auxiliary coordinate system defined through X*, Y* and Z*- Fig. 8.

The displacement mapping principle is based on find and compares the changes in each facet in the current image with the reference image (without deformation).

The time-varying distortion may be defined at each pixel location (x_s, y_s) by a time-dependent velocity function, $v(x_s,y_s;t)$. Using finite difference or another appropriate method to estimate $v(x_s,y_s;t)$, the drift displacement correction at each pixel can be obtained by the integration of v over time [16].

For a set of 3D measurements, we use two cameras previously calibrated; the surface must be within the calibrated 3D space. Images are recorded (cameras right and left) at various deformation stages.

During the measurement, ARAMIS compares different facets that are identified and followed through their individual gray level. Fig. 9 displays the variation in pixels position following the green line (deformed state) and the white line that represents the undeformed state of the facet analysed.

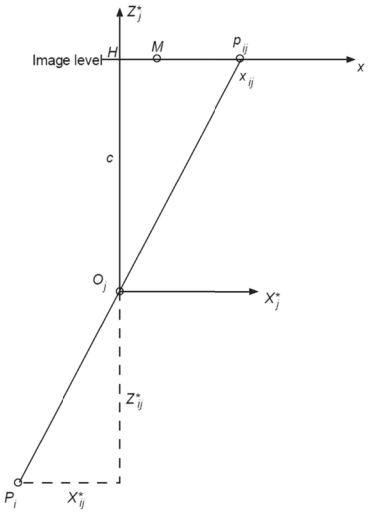

Fig. 8. Geometric model of the central projection [16]

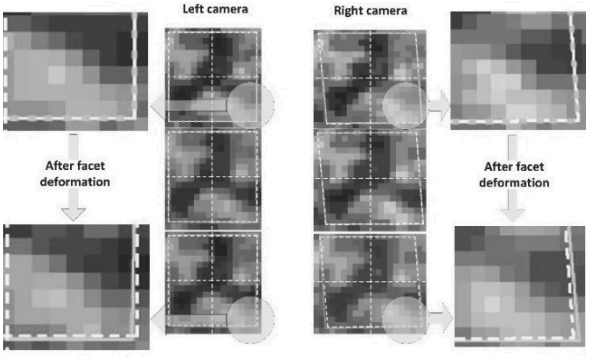

Fig. 9. Comparative analysis between the pixels initial position (white line) and pixels position after deformation (dashed green) [13]

3. Direct measurement system

3.1. The direct measurement system summary description

Non-destructive testing (NDT) characterizing material thickness, integrity or other physical properties by means of high frequency sound waves has become a widely used technique in quality control [19]. In thickness measurement, ultrasonic techniques permit a rapid and reliable measurement of thickness without requiring access to both sides of a part. An accuracy as high as ± 1 micron is achievable in some applications. On-line or in-process measurement of extruded plastic sheeting is often possible [18].

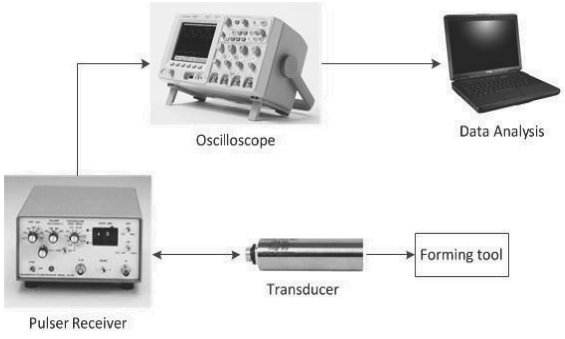

Fig. 10. Experimental setup schema of the direct measurement system

Ultrasonic thickness measurement generally operates at frequency 20 MHz, using a piezoelectric transducer to generate bursts of sound waves when excited by electrical pulses. Higher frequencies (> 20 MHz) are recommended to optimize the resolution of finer not attenuating and non-scattering materials. Fig. 10 shows the experimental setup used to measure the bulge thickness during the forming process.

The experimental setup also consists of a pulser receiver Panametrics NDT® model 5077PR to generate and to capture the voltage pulse applied to the transducer. A digital oscilloscope Agilent Technologies® model DSO5012A, was used to digitize the signal received that is recorded for digital signal processing.

3.2. Ultrasonic thickness technique

A pulse-echo ultrasonic thickness technique determines the thickness of the bulge by accurately measuring the time required for a short ultrasonic pulse generated by the transducer to travel through the thickness of the material, reflect from the back and be returned to the transducer.

In this application, this time interval is only a few microseconds. The measured two-way transit time is divided by two to account for the down-and-back travel path, and then multiplied by the velocity of the sound of the tested material. The result is expressed in the relationship:

$$t = v.T_f/2 \tag{25}$$

Where t is the length in the thickness direction of the test piece, v is the velocity of sound waves in the material, and T_f is the measured delay time.

Measurements are made between two successive back wall echoes, using direct contact transducers with a Vaseline couplant layer. This mode is employed because there is a clean multiple back wall echoes appearance, which typically limits its use to materials of relatively low attenuation and high acoustic impedance such as Pb-Sn alloy. While using this mode is possible regarding the tested material, it offers the highest measurement accuracy and the best minimum thickness resolution.

Fig. 11 shows samples of voltage amplitude signals at different stages of the forming process obtained using the experimental setup described previously.

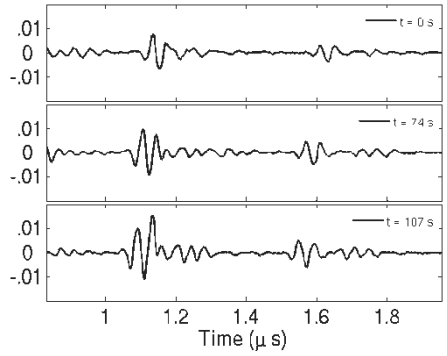

Fig. 11. Three samples of a-scan obtained using pulse-echo mode showing the first and second reflection at different time steps

3.3. Accurate resolution of echo detection

Basically, the idea is to calculate the time difference at which each echo occurs. Instead of using peak-detection or threshold detection which relies only on a unique point over the time sequence, the cross-correlation is based on multiple points of the wave packages. The cross-correlation method is applied to detect the time-of-flight between two successive back wall echoes. In signal processing, auto-correlation is the cross-correlation of a signal with itself.

$$R(\tau) = \int_{-\infty}^{\infty} f(t)f(t-\tau)dt \tag{26}$$

In practice, the time-of-flight, T_{f0}, can be estimated by finding the peak of auto-correlated signals. This happens because the lag τ relates to the time-of-flight, as the maximum positive correlation occurs indicating the arrival of the reflected echo.

Fig. 12 shows the auto-correlated signals from Fig. 11, obtained by using a discrete time approximation of equation (26). A vertical line annotation indicates the calculated time-of-flight in each graph, showing a decrease as the thickness changes over time.

3.4. Thickness reduction calculation

The percentage of thickness reduction during a material thinning process is defined as TR. Considering equation (25), the relationship between thickness reduction and the measured time-of-flight is

$$TR = (t_0 - t)/t_0 = (T_{f0} - T_f)/T_{f0} \tag{27}$$

Where t and t_0 represent the current and the initial length in the thickness direction; T_f and T_{f0} represent the current and initial measured time-of-flight, respectively. As the thickness reduction calculation does not depend on the knowledge of mechanical properties, the term of the sound wave velocity can be dropped in equation (27). Fig. 12 shows normalized TR to ignore the energy influence in this comparison.

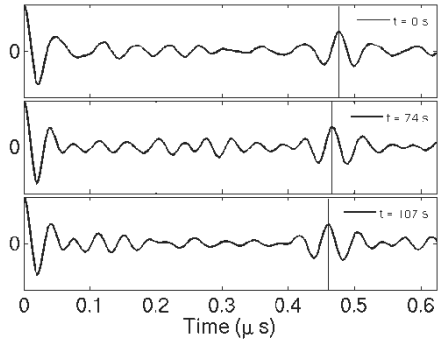

Fig. 12. Normalized auto-correlation of a-scan signals showing the time-of-flight detection for each a-scan

4. Experimental methodology

A Pb-Sn60 (40% Pb and 60% Sn) laboratory cast ingot was conventionally rolled, and circular blanks (260 mm diameter) were machined from the sheet.

The test was performed at room temperature using compressed air, since the league has no oxidation problems. Fig. 13 shows a photograph of the bulge test tool fabricated in steel ABNT 1045. The blank is inserted between the base and the blank holder.

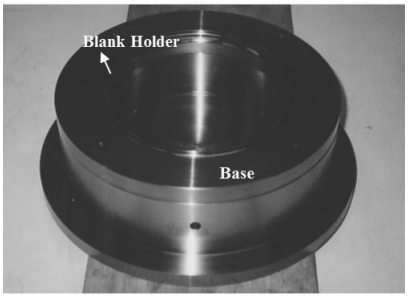

Fig. 13. The bulge test tooling

The bulge test was conducted at room temperature and a constant pressure curve was applied. Based on that, the material parameters were not the intention of this work, which does not mean to reach specific forming conditions.

The ARAMIS 5M measurement system, whose setup is shown in Fig. 13, was calibrated to measure with a frame rate of one image per second. Equipped with a 23 mm lens and a 175x140 square calibration object, the system should be able to achieve a measuring volume of 200x170 mm; however, the measure distance recommended - 530 mm - was increased to 600 mm before calibrating, and the measuring area reached the diameter of 240 mm after calibrating.

Fig. 14 shows the setup of the bulge tests with the GOM-ARAMIS.

A second step of the experimental setup was to include the indirect measure system and place the ultrasound transducer at the dome height, as shown in Fig. 15. A NDT transducer model KB-AEROTECH Alpha with 25 MHz central frequency was used to measure the thickness reduction of the bulge dome.

5. Experimental results

In order to better understand the time dependent analyses, two steps were chosen and individually presented, step 75 and step 107. For each step, direct and indirect measurements were confronted. Along the main measurement section, seven points were monitored during the bulge test six points were obtained through DIC and the last one was obtained by a pulse-echo ultrasonic measurement system.

Fig. 14. Setup of the bulge tests with the GOM-ARAMIS

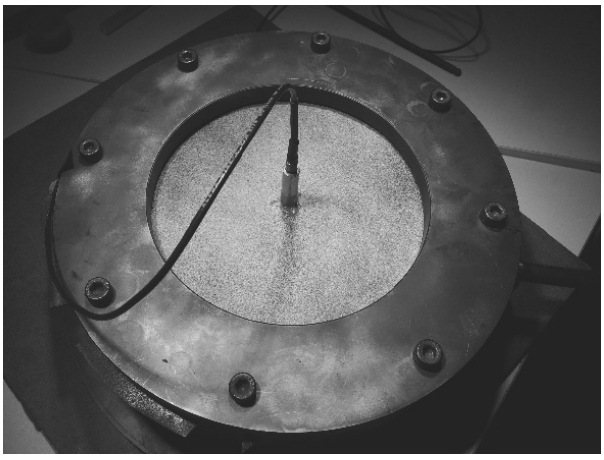

Fig. 15. Setup of the bulge tests with an ultrasound transducer

Fig. 16 exemplifies both measurement systems acting at the same time.

a)

b)

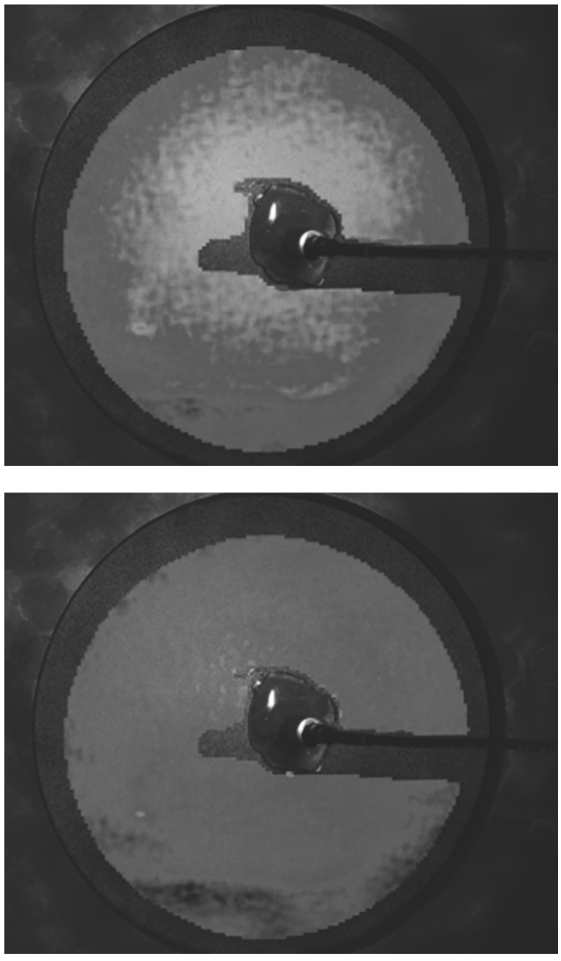

Fig. 16. GOM Aramis Image at bulge test at T = 107s (a) T = 75 s (b)

Fig. 17a, b localize the stage points and represent the position of the ultrasonic transducer.

a)

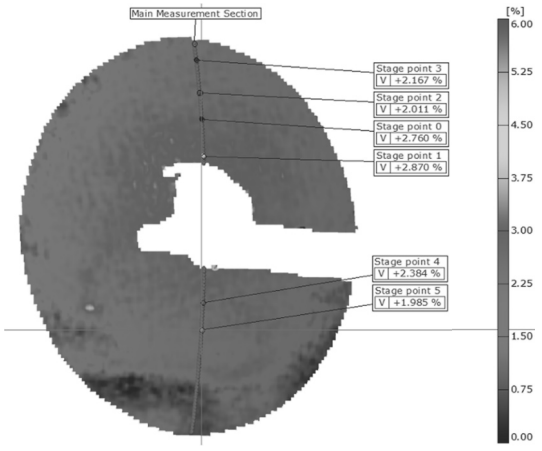

b)

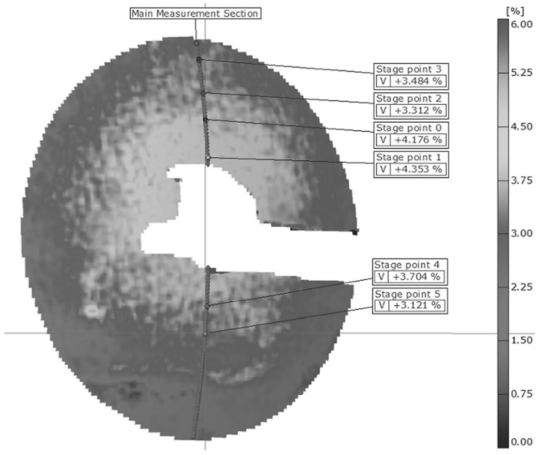

Fig. 17. Thickness reduction by DIC of bulge test at time step T= 75 s (a) and T=107s (b)

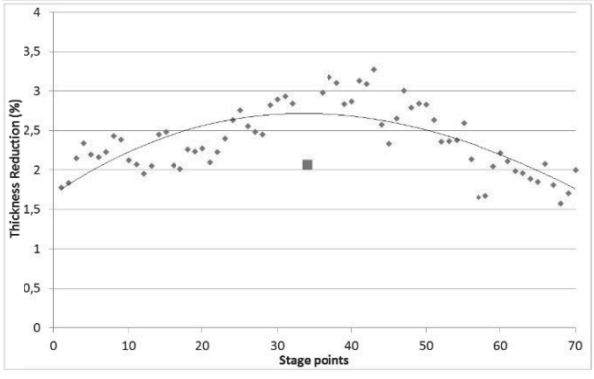

Fig. 18. Thickness reduction result at the main measurement section by DIC and ultrasonic transducer of bulge test at time step T=75 s

Figs. 18 and 19 locate the direct measurement result (the largest square marker) in between the indirect measurement results (the smallest ones) obtained by the DIC system. The former image shows the thickness reduction result at the main measurement section by DIC and ultrasonic transducer of bulge test at time step T=75s, and the latter shows the thickness reduction result at the main measurement section by DIC and ultrasonic transducer of bulge test at time step T=107s.

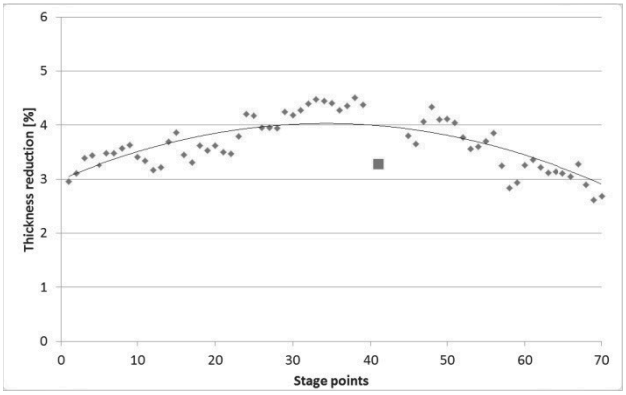

Fig. 19. Thickness reduction result at the main measurement section by DIC and ultrasonic transducer of bulge test at time step T = 107 s

To complete the analysis, the thickness reductions are presented for all the seven points monitored during the bulge test all over the time, as shown in Fig. 20.

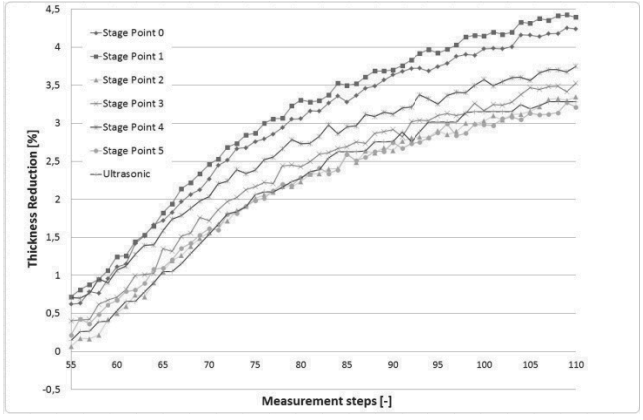

Fig. 20. Thickness reductions for all the seven points monitored during the bulge test all over the time

6. Conclusions

An indirect method, Digital Image Correlation (DIC), is compared with a direct one, ultrasound pulse-echo method, in situ, real time and on the same specimen.

The results shown in Figs. 18 and 19 are two examples of the comparison between the direct and indirect measurements. In both

of them it is possible to note that the difference between the tendency curve of the indirect results and the direct measurement are approximately 0.5 % of thickness reduction.

The ultrasound pulse-echo method has the resolution of 1.5 μm and the DIC has the resolution of 1 μm.

Based on the resolution of the measurement systems, and the constant difference between the tendency curve of the indirect results and the direct measurement over time, the comparison between the direct and indirect measurement systems is validated.

Fig. 20 represents the time behaviour agreement for the monitored points, the six-stage point (0-5) and the ultrasonic measurement point.

References

[1] Y. Chen, K. Kibble, R. Hall, X. Huang, Numerical analysis of superplastic blow forming of Ti-6Al-4V alloys, Materials and Design 22 (2001) 679-685.

[2] V. Gagov, N. Feschiev, D.S. Comsa, E. Minev, Strain hardening evaluation by bulge testing of sheet metals, Proceedings of the 12th International Scientific Conference on "Achievements in Mechanical and Materials Engineering", Gliwice, 2003.

[3] P. Guanabara Jr., L.O. BUENO, Assessing the superplastic behaviour of a Fe-Mn-Al austenitic stainless steel. Proceedings of the 61th Annual Congress ABM, Associação Brasileira de Metalurgia e Materiais, 2006, 2654-2663.

[4] B. Tomov, V. Gagov, E. Yankov, R. Radev, Research highligths of sheet metal testing by hydraulic bulging, Journal of Achievements in Materials and Manufacturing Engineering 46/1 (2011) 65-70.

[5] J. Cheng, The determination of material parameters from superplas-tic inflation test, Journal of Materials Processing Technology 58 (1996) 233-246.

[6] P. Guanabara Jr., G.F. Batalha, Conformação superplástica e otimização dos parâmetros do material - uma breve revisão. In: 64º Anual Congress ABM, Associação Brasileira de Metalurgia e Materiais-ABM, 2009, 1.

[7] Y. Aoura, Contribution a la modélisation du comportement super-plástique des alliages métalliques pour les procédés de mise em forme, Tesis presented at École Nationale Supérieure d'Arts et Métiers, 2004.

[8] B. Baudelet, J. Lian, A composite model for superplasticity, Journal of Materials Science 30 (1995) 1977-1987.

[9] G.L. Damoulis, G.F. Batalha, New trends in sheet metal forming analysis and optimization trough the use of optical meas-urement technology to control springback, International Journal of Material Forming 3 (2010) 29-39.

[10] K.A. Fowler, G.M. Elfbaum, K.A. Smith, T.J. Nelligan, Theory and application of precision ultrasonic thickness gauging, Insight 38 (1996) 582 -592.

[11] E.P. Marinho, A. Sakata, E.F. Prados, G.F. Batalha, Instrumentation and Control of a Bulge Test on a Superplastic Pb-Sn Alloy, Trans Tech Publications, Materials Science Forum 735 (2013) 224-231.

[12] S. Tománek, V. Kafka, Non-contact Deformation Measurement by ARAMIS Photogrammetry System, Aerospace Proceedings, Prague, 1 (2006) 13-17.

[13] GOM mbH. ARAMIS user Manual - Software, ARAMIS 6.1 and higher, Braunschweig, Germany, 2009.

[14] B. Stier, S. Reese, Verification of an optical metrology system (ARAMIS) by comparing experimental data with FE calculations and continuum approaches, Proceedings in Applied Mathematics and Mechanics 11 (2011) 289-290.

[15] G. Giuliano, Thickness and strain rate at the sheet dome apex in superplastic bulge forming tests, Proceedings of the 12th International Esaform Conference on Material Forming, Italy, 2009.

[16] M.A. Sutton, J.J. Orteu, H.W. Schreier, Image correlation for shape, motion and deformation measurements, Springer Publishing Company, 2009.

[17] M. Vulcan, Der pneumatische tiefungsversuch und seine anwendug in der superplastischen aluminium-blechumformung, Doctor of Engineering Thesis, University of Stuttgart, Germany, 2006, 108.

[18] S. Dejardin, J.C. Gelin, S. Thibaud, On-line thickness measurement in incremental sheet forming process, Proceedings of the 13th International Conference on Metal Forming, Toyohashi 19-22, 2010, 938-941.

[19] G.F. Batalha, M. Stipkovic, C.E.V. Salazar, Analysis of the contact conditions and its influence on the interface friction in forming process, Proceedings of the International Conference on Metal Forming, Balkema, Rotterdam, 2000.